JFM RAPIDS
journals.cambridge.org/rapids

Elastically induced turbulence in Taylor–Couette flow: direct numerical simulation and mechanistic insight

Nansheng Liu[1,2] **and Bamin Khomami**[1,†]

[1]Materials Research and Innovation Laboratory, Department of Chemical and Biomolecular Engineering, University of Tennessee, Knoxville, TN 37996-2200, USA

[2]Department of Modern Mechanics, University of Science and Technology of China, Anhui, Hefei 230026, China

Direct numerical simulation (DNS) of elastically induced turbulent flows has posed great challenges to researchers engaged in developing first-principle models and simulations that can predict faithfully the complex spatio-temporal dynamics of polymeric flows. To this end, DNS of elastically induced turbulent flow states in the Taylor–Couette (TC) flow are reported here with the aim of paving the way for a mechanistic understanding of this new class of flows. Specifically, the DNS not only faithfully reproduce the key feature of elastically induced turbulent flows, namely, substantial excitation of fluid motion at the smallest temporal and spatial scales, but also for the first time demonstrate the existence of three distinct flow regions in the gap for the inertio-elastic turbulence state: (i) a fluid-inertia (or outflow-) dominated inner-wall region; (ii) a fluid-elasticity (or inflow-) dominated outer-wall region; and (iii) an inflow/outflow core region. Based on this observation, a simple mechanism for the inertio-elastic turbulence in the TC flow has been postulated.

1. Introduction

In 1990, a purely elastic instability at vanishingly small Reynolds number, *Re*, and $O(1)$ Weissenberg number, *We*, in the Taylor–Couette (TC) flow of dilute polymeric solutions was experimentally observed. Moreover, it was demonstrated that this instability occurs due to significant macromolecular stretching around curved streamlines and the consequent development of large elastic 'hoop' stresses. Under these conditions, infinitesimal perturbations to the flow field will result in an unstable stratification of 'hoop' stresses and flow instability. The secondary flow state is

† Email address for correspondence: bkhomami@utk.edu

composed of stationary vortices stacked along the axis of the rotating inner cylinder (Larson, Shaqfeh & Muller 1990; Larson 1992; Shaqfeh 1996).

Following the aforementioned discovery, much research was devoted to accurate prediction of the instability onset conditions (Larson *et al.* 1990; Larson 1992; Su & Khomami 1992; Shaqfeh 1996). However, isothermal linear and nonlinear stability analyses identified a non-stationary antisymmetric mode of instability with a critical *We* that was an order of magnitude greater than the experimentally measured value (Larson *et al.* 1990; Avgousti & Beris 1993; Sureshkumar, Beris & Avgousti 1994). After a decade of further studies, it was demonstrated that the interplay between viscous dissipation and the thermal sensitivity of the high-viscosity dilute polymeric solutions used in the experimental studies significantly decreases the disturbance dissipation rate, leading to flow destabilization at *We* lower than that of the corresponding isothermal flow. In fact, the prediction of the non-isothermal linear stability analysis (Al-Mubaiyedh, Sureshkumar & Khomami 1999, 2000) was found to be in excellent agreement with the experimentally observed onset conditions, i.e. axisymmetric stationary vortices and $O(1)$ *We* (White & Muller 2000, 2002*a*,*b*).

In the past decade, higher-order nonlinear flow transitions in viscoelastic TC flow have also been extensively studied. Specifically, Groisman & Steinberg (1996, 1997, 1998) observed three dominant flow patterns in dilute PAAm aqueous solutions at high *We* and $O(1)$ elasticity number, $E \equiv We/Re$, namely, diwhirls (DW), oscillatory strips (OS) and disordered states (DO). Subsequently, these flow patterns were reproduced via hi-fidelity direct numerical simulations (DNS) (Thomas, Sureshkumar & Khomami 2006*b*; Thomas, Khomami & Sureshkumar 2009), i.e. the *We* and *E* corresponding to transition from one flow state to another were faithfully reproduced.

More recently, Dutcher & Muller (2009, 2011, 2013) have thoroughly examined higher-order flow transitions in viscoelastic TC flow with a series of well-characterized dilute PEO aqueous solutions. In particular, their studies have clearly demonstrated elastic modification of the well-known Newtonian TC flow states even at small *E*, including 'turbulent like' flows dubbed 'elastically dominated turbulence' that exhibit broad spatial and temporal frequencies at $E \sim 0.1$–0.2 and $Re \sim 180$–207 (Dutcher & Muller 2013). Moreover, Latrache, Crumeyrolle & Mutabazi (2012) have experimentally investigated transition to turbulence in flow of a semidilute shear-thinning PEO solution at low $E \sim 0.01$–0.05. Specifically, they observed a flow state with a high degree of spatio-temporal intermittency followed by inertio-elastic turbulence, where the later is characterized by inflow/outflow strips arranged randomly in the time–space plots.

Groisman & Steinberg (2004) have also detected flow states with broad temporal frequency spectra in TC flow of PAAm dilute solutions in the limit of vanishing *Re* and $We_c \sim 5$ (very large *E*), dubbed 'elastic turbulence'. Specifically, they observed broad frequency spectra in the radial velocity with two power-law decay regimes of slope -1.1 and -2.2 at low and high frequencies, respectively. In addition, it was shown that the probability density function (PDF) of the radial velocity at the middle of the gap exhibited a weakly asymmetric shape instead of the Gaussian distribution.

Although numerical simulation of an elastically driven flow transition from a stationary to randomly fluctuating states at vanishing *Re* and $O(1)$ *We*, has been recently performed, the computations are confined to two-dimensional or three-dimensional periodic Kolmogorov flows excited by an external forcing (Berti *et al.* 2008; Berti & Boffetta 2010; Zhang *et al.* 2013). Hence, the detailed flow–microstructure coupling needed for elucidating the mechanism of 'elastically

induced turbulence' is still lacking. To this end, the goal of this study is to perform the first three-dimensional DNS of elastically induced turbulence in TC flow, and ultimately to pave the way for a mechanistic understanding of this new class of flows.

2. Problem formulation

To perform DNS of the 'elastically induced turbulent' flow state we have modified our fully spectral, three-dimensional parallel algorithm used earlier to elucidate higher-order nonlinear flow transitions in viscoelastic TC flow (Thomas *et al.* 2006*b*, 2009). In accord with our prior studies of polymer-induced turbulent drag reduction (Li, Sureshkumar & Khomami 2006), the FENE-P (finitely extensible nonlinear elastic-Peterlin) constitutive equation is used to model the polymer contribution to the total stress. We have chosen $d = R_2 - R_1$, $d/(R_1\Omega)$, $R_1\Omega$, $\rho(R_1\Omega)^2$, and $\eta_P R_1\Omega/d$ as scales for length, time, velocity $\boldsymbol{u}$, pressure p, and polymer stress $\boldsymbol{\tau}$, respectively. In these equations R_1 and R_2 correspond to the inner and outer cylinder radii, respectively, Ω denotes the inner cylinder angular velocity, ρ represents the solution density, and the total solution viscosity η_T is the sum of the solvent (η_S) and polymeric (η_P) contributions. Further, we scale the conformation tensor $\boldsymbol{C}$, which represents the ensemble average of the second moment of the end-to-end vector of the polymer chain, with respect to kT/H, where k, T, and H denote the Boltzmann constant, absolute temperature, and Hookean spring constant of the elastic dumbbell model, respectively. The resulting dimensionless equations governing the motion of an incompressible FENE-P fluid are as follows:

$$\frac{\partial \boldsymbol{u}}{\partial t} + \boldsymbol{u} \cdot \nabla \boldsymbol{u} = -\nabla p + \frac{\beta}{Re}\nabla^2 \boldsymbol{u} + \frac{1-\beta}{Re}\nabla \cdot \boldsymbol{\tau} \qquad (2.1)$$

and

$$\frac{\partial \boldsymbol{C}}{\partial t} = -\boldsymbol{u} \cdot \nabla \boldsymbol{C} + \boldsymbol{C} \cdot \nabla \boldsymbol{u} + (\nabla \boldsymbol{u})^{\mathrm{T}} \cdot \nabla \boldsymbol{C} - \boldsymbol{\tau} \qquad (2.2)$$

where $\boldsymbol{\tau} = \{(L^2 - 3)/[L^2 - \mathrm{trace}(\boldsymbol{C})]\boldsymbol{C} - \boldsymbol{I}\}/We$ and $\beta = \eta_S/\eta_T$, and L is the maximum chain extensibility; $Re = \rho R_1\Omega d/\eta_T$ and $We = \lambda R_1\Omega/d$ where λ is the polymer relaxation time. These equations are also supplemented by no-slip boundary conditions at the walls, as well as periodic boundary conditions in the z direction. In addition, a diffusive term $\kappa\nabla^2\boldsymbol{C}$ is added to (2.2) in the bulk flow region to numerically stabilize the integration of the conformation tensor evolution equation. In order to retain the essential dynamics resulting from flow–microstructure coupling while maintaining numerical stability, the value of scalar stress diffusivity κ must be chosen as low as possible (Sureshkumar & Beris 1995; Thomas *et al.* 2006*a*, 2009). Moreover, we have employed a time-adaptive scheme for selecting the value of κ, which corresponds to a numerical Schmidt number $Sc_\kappa^{-1}[=(\kappa Re)]$ with maximum of $O(10^1)$ in all simulations. It should also be noted that the original constitutive equation without the diffusive term is applied at the walls, thus no boundary conditions are imposed at the walls for $\boldsymbol{C}$. We use a large value for L, $L^2 = 10\,000$, and $\beta = 0.8$ for which the polymeric solution has a nearly shear-independent viscosity, and $\eta = R_1/R_2$ is set at 0.8, the same value used in our previous simulations for higher-order viscoelastic TC flow transitions (Thomas *et al.* 2006*b*, 2009).

Similar to the experimental findings of Dutcher & Muller (2009, 2013) where $\eta = 0.912$, our DNS at $Re = 250$ and $We = 50$ ($E = 0.2$) gives rise to a turbulent-like flow state that is labelled inertio-elastic turbulence (Latrache *et al.* 2012). These
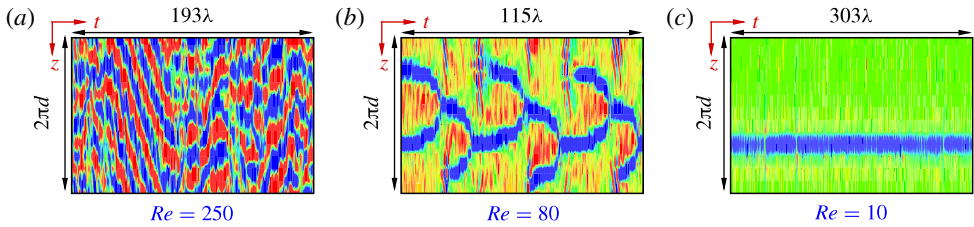
FIGURE 1. Space–time plots of radial velocity u_r at the middle of the gap along an axial (z) line passing through $\theta = \pi$: (*a*) inertio-elastic turbulence, (*b*) flame-like turbulent OSs, and (*c*) a 'solitary' turbulent OS. The blue and red regions correspond to radial inflows ($u_r < 0$) and outflows ($u_r > 0$), respectively.

results have been generated by using an initial condition composed of the steady base flow plus a divergence-free velocity fluctuation in addition to perturbation of the eigenvalues of **C**. The critical value of *Re* for the onset of Taylor vortex flow (TVF) in the flow geometry under consideration, i.e. $Re_{c\_TVF}^{Newtonian}$, is approximately 80 (Groisman & Steinberg 1998; Dutcher & Muller 2009, 2013). At $Re = 250$, the Newtonian flow is that of a modulated wavy vortex flow, while elastic turbulence for a dilute polymeric solution at $E = 0.2$ has been observed (Dutcher & Muller 2009, 2013). To examine the nonlinear flow transitions at $Re < 250$ for which Newtonian TVF and purely azimuthal flows are expected, we have gradually decreased *Re* from 250 to 10, in discrete steps while maintaining *We* fixed at 50. Correspondingly, *E* increases from 0.2 to 5. For each *Re*, the simulation is performed for a sufficiently long time (typically of $O(100\lambda)$) and the final solution is used as an initial condition for the simulation at the next *Re*. In each case, after a 'statistically steady' flow state is realized, the flow statistics are calculated by ensemble averaging over ∼40λ.

3. Results and discussion

Decreasing *Re* from 250 to 10 results in a flow transition pathway from an inertio-elastic turbulence state to flows characterized by a coexistence of spatially localized coherent structures and temporally fluctuating (random) fluid motion (see figure 1). Specifically, we observe three turbulent flow states, i.e. inertio-elastic turbulence at $Re > Re_{c\_TVF}^{Newtonian}$ (see figure 1*a*), flame-like patterns made up of merging and splitting OSs at $Re \approx Re_{c\_TVF}^{Newtonian}$ (see figure 1*b*), and a 'solitary' OS at $Re < Re_{c\_TVF}^{Newtonian}$ (see figure 1*c*). In figure 1, the blue and red regions correspond to radial inflows ($u_r < 0$) and outflows ($u_r > 0$), respectively. In the inertio-elastic turbulence state (see figure 1*a*), strong radial inflows (blue) and outflows (red) appear randomly in the space–time plots, indicating existence of fluctuating fluid motions with a broad range of temporal scales. Similar flow states dubbed 'elastically dominated turbulence' have also been experimentally identified by Latrache *et al.* (2012) and by Dutcher & Muller (2013). These random inflows/outflows occur on time scales that are much greater than the fluid relaxation time. Hence, one does not observe a dominant characteristic time scale in this flow regime. On the other hand, for the flame-like OSs (see figure 1*b*), the time period for the merging and splitting of the oscillatory strips is ∼43λ. Each merging/splitting cycle begins with a highly localized rotating standing wave followed by formation of a new strip of strong radial inflow above or below the existing strip. Consistent with experimental findings (Baumert & Muller 1997, 1999), these two strips are in turn convected axially upwards/downwards and eventually coalesce into
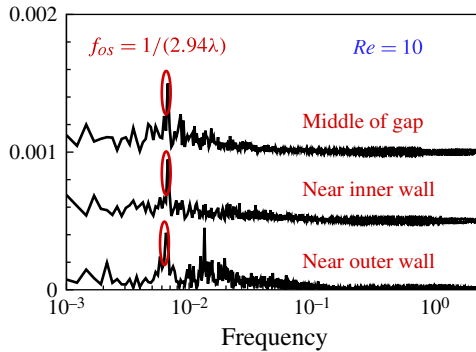
737 R4-4

FIGURE 2. PSDs of radial velocity u_r for the 'solitary' turbulent OS state at the middle of the gap, as well as near the inner and outer walls. The PSDs have been shifted appropriately in the ordinate direction for clarity.
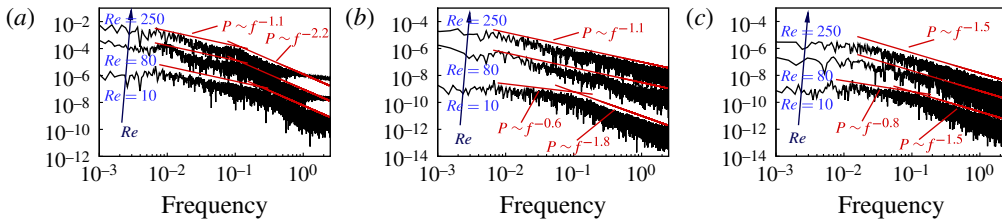

FIGURE 3. PSDs of radial velocity u_r: (*a*) at the middle of the gap, (*b*) near the inner wall, and (*c*) near the outer wall. For clarity, the PSDs for $Re = 80$ and 10 have been shifted downward by 2 and 4 logarithmic scales, respectively.

a single strip. In the 'solitary' OS flow state (see figure 1*c*), high-frequency random u_r-fluctuations are superimposed on low-frequency oscillations of the axially localized inflow strip. The low-frequency oscillation of the inflow strip is evident from a peak in the power spectral densities (PSD) of u_r at $f_{OS} \approx 1/(2.94\lambda)$ (see figure 2). It should also be noted that this flow pattern is different from the periodically oscillating flow patterns, i.e. non-axisymmetric OS (flames), axisymmetric OS, and DW, observed in our earlier studies (Thomas *et al.* 2006*b*, 2009). Specifically, this flow state contains high-frequency fluctuating fluid motions that coexist with spatially highly ordered coherent structures.

The influence of nonlinear flow–microstructure coupling on the fluctuating fluid motion can be quantified by examining the power spectra of the radial velocity u_r. Overall, u_r-PSDs exhibit broad continuous power-law-decay regions spanning more than two orders of magnitude in frequency, indicating substantial excitation of random-like fluid motion at the smallest temporal and spatial scales (see figure 3), a key feature of elastic turbulence (Groisman & Steinberg 2004; Dutcher & Muller 2009, 2013). Specifically, at the middle of the gap (see figure 3*a*), the experimentally measured u_r-PSDs (Groisman & Steinberg 2004) are reproduced accurately, i.e. two continuous regions with power-law-decay exponents of -1.1 and -2.2 at low and high frequencies are observed. The self-similar nature of u_r-PSDs at the middle of the gap (see figure 3*a*), indicates a weak dependence of the fluctuating fluid motion on E. This trend is also in qualitative agreement with experimental findings (Groisman
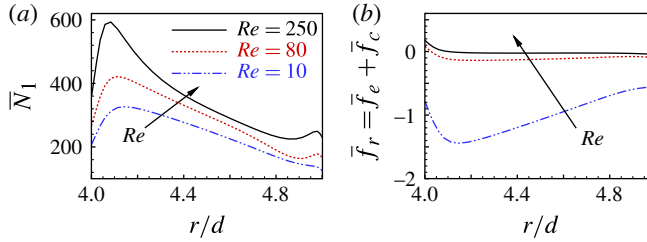
737 R4-5

FIGURE 4. Ensemble-averaged first normal stress difference (N_1) (*a*) and radial driving force (f_r) (*b*) across the gap. Here, f_r is the sum of the elastic body force $f_e = -(1 - \beta)/Re \times N_1/r$ (where $N_1 = \tau_{\theta\theta} - \tau_{rr}$ and $\tau_{\theta\theta}$ is the 'hoop' stress) and the centrifugal force $f_c = u_\theta^2/r$. The over-bar denotes ensemble averaging in time and in the (θ, z) plane.

& Steinberg 2004). The fluctuating fluid motion in the wall regions, however, exhibits variation with E (see figure 3*b,c*). In fact, u_r-PSDs of the inertio-elastic turbulence ($Re = 250$) are reminiscent of those of the flame-like turbulent OSs ($Re = 80$) in the wall regions, i.e. a single decay region with power-law-decay exponent of -1.1 and -1.5 exists near the inner and outer walls, respectively (see figures 3*b* and 3*c*). This close correspondence of the power-law-decay exponents of u_r-PSDs points to qualitatively similar fluctuating fluid motion in the inertio-elastic turbulence and flame-like turbulent OSs flow states in the wall regions. Interestingly, a power-law-decay exponent of -1.5 has also been observed by Bonn *et al.* (2011) in their experiments on viscoelastic jet flows into a cylindrical tube, indicating a direct cascade of energy to small scales with practically no intermittency. By contrast, in the 'solitary' turbulent OS ($Re = 10$) flow state, u_r-PSDs near the inner and outer walls exhibit two continuous power-law-decay regions at low and high frequencies that are distinctly different from those observed in the middle of the gap. These characteristics of the u_r-PSDs clearly demonstrate that strong flow–microstructure coupling gives rise to fluctuating fluid motions with self-similar dynamics in the middle of the gap that are distinct from the near-wall fluctuating flow dynamics. This striking difference can be rationalized in terms of the significant variation in polymer extension and the corresponding polymer body force across the gap, i.e. polymer stress boundary layer formation in the wall regions (see figure 4*a*). Specifically, consistent with earlier experimental findings on elastic turbulent flows (Burghelea, Segre & Steinberg 2007; Jun & Steinberg 2011), a very rapid increase of elastic stress within the boundary layer is observed (see figure 4*a*). However, the saturation of elastic stresses in the bulk observed in curvilinear channel and swirling elastic turbulent flows is not seen in our inertio-elastic TC flow, i.e. a notable stratification of hoop stresses is indicated near the centre of the gap.

Although u_r-PSDs in the wall regions suggest a similarity of the fluctuating fluid motion in the inertio-elastic turbulent and flame-like turbulent OSs flow states, a closer examination of the flow dynamics via u_r-PDFs shown in figure 5 underscores fundamental difference in u_r-statistics between these two flow states. These differences mainly arise due to the axial localization of coherent structures in the latter flow. Thus, u_r-PDFs for the flame-like turbulent OSs ($Re = 80$) and a 'solitary' turbulent OS ($Re = 10$) have similar characteristics, i.e. u_r-PDFs with a long tail at negative u_r and a maximum at $u_r > 0$ are observed at the middle of the gap and in the wall regions (see figure 5*a–c*). This characteristic signature of u_r-PDFs originates from the striking asymmetry between the strong inflows occurring in the narrow cores of OSs
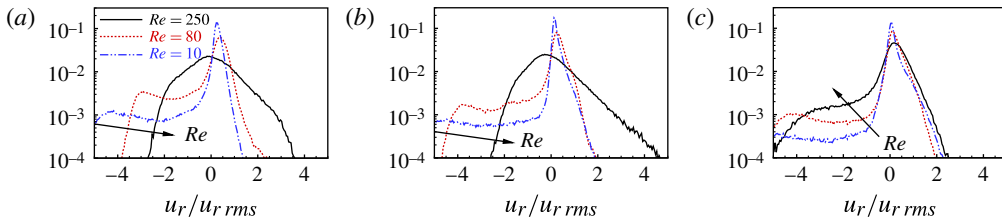
737 R4-6

FIGURE 5. Probability density functions (PDFs) of radial velocity u_r: (*a*) at the middle of the gap, (*b*) near the inner wall, and (*c*) near the outer wall.

wherein significant polymer extension is realized, and the much weaker outflows that spread axially over a wide region surrounding the OS-occupied zones (Groisman & Steinberg 1998). The inflow-skewed (or negative-u_r-skewed) asymmetry is one of the key characteristics of the elasticity driven flow states (DW, OS and DO) (Groisman & Steinberg 1998; Kumar & Graham 2000). Hence, the dynamics of the fluctuating fluid motion in these flow states, i.e. flame-like and 'solitary' OS, are essentially driven by polymeric elastic forces (inflow-dominated). However, at lower E where inertio-elastic turbulence is realized ($Re = 250$) a very different u_r-PDF profile is observed, namely, a long tail at positive u_r indicating an outflow-dominated regime at the middle of the gap (see figure 5*a*) and near the inner wall (see figure 5*b*), and a long tail at negative u_r indicating an inflow-dominated regime near the outer wall (see figure 5*c*).

The underlying physics of the above-mentioned r-dependence of u_r-PDFs for inertio-elastic turbulence can be scrutinized by a direct examination of the relative importance of the elastic body force f_e and the centrifugal force f_c (see figure 4*b*). Specifically, in this flow state ($Re = 250$), near the inner wall $f_e \approx -0.08$ and $f_c \approx 0.25$. Hence, in this region, the resultant radial driving force f_r is radially outward, indicating a centrifugally (or inertially) dominated regime. As a result, coherent structures composed of centrifugally driven strong outflows ($u_r > 0$) localized in axially narrow regions that are surrounded by much weaker inflows are generated (see figure 6*a*ii). This in turn results in the outflow-skewed asymmetric u_r-PDFs shown in figure 5(*b*). On the other hand, near the outer wall the elastic body force is ~-0.04 while the centrifugal force approaches zero (see figure 4*b*). Hence, the radially inward force in this elastically dominated flow region drives an elastic instability which gives rise to localized strong inflows and commensurate fluctuating motions. The corresponding velocity disturbances are in turn convected inwards as evinced by the localized strong inflows depicted in figure 6(*a*iii) and by the resulting inflow-skewed asymmetric u_r-PDF depicted in figure 5(*c*). Therefore, the occurrence of inertio-elastic turbulence can be mechanistically ascribed to the onset of near-outer-wall elastic instability and the resulting fluctuating velocities, which ultimately lead to a substantial excitation of turbulent-like fluid motion in the entire gap (see figure 3). Moreover, in the gap centre, the weakly asymmetric u_r-PDF at $Re = 250$ (see figure 5*a*) and the small negative f_r of ~-0.01 (see figure 4*b*) clearly underscore the balance between elastic and inertial forces that leads to the appearance of localized outflows and inflows originating from the inner- and outer-wall regions, respectively.

Significant polymer extension is a pre-requisite for elastic instabilities and the resulting highly localized strong inflows in the outer-wall region. To this end, the polymer extension and the resulting flow structure modifications have been examined via visualization of the instantaneous inflow/outflow streaks. For the inertio-elastic turbulence (see figure 6*a* i–iii), disordered inflow/outflow streaks indicate an irregular
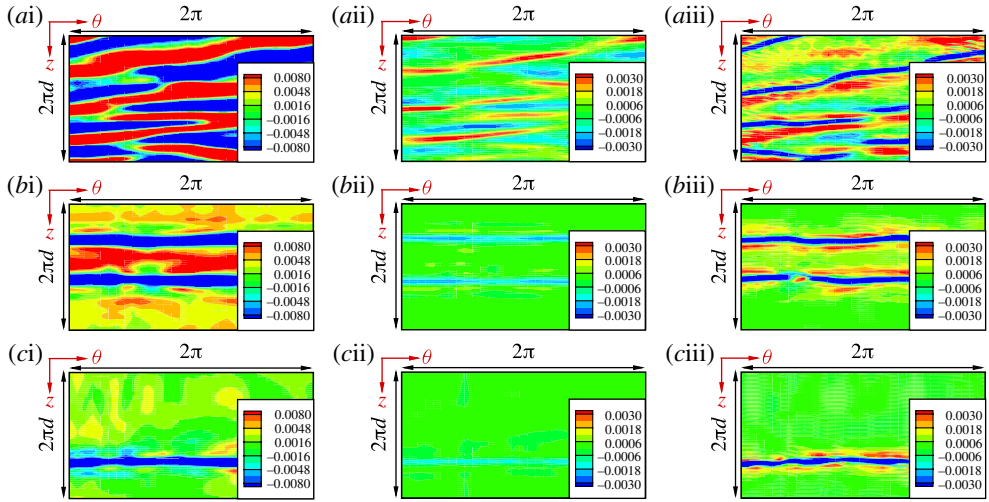
737 R4-7

FIGURE 6. Instantaneous contour plots of radial velocity u_r: columns (i), (ii) and (iii) depict contours at the middle of the gap, near the inner and outer walls, respectively; and rows (*a*), (*b*) and (*c*) depict $Re = 250$, $Re = 80$, and $Re = 10$, respectively.

spatial arrangement of regions with significant polymer extension. On the other hand, for the flame-like turbulent OSs (see figure 6*b* i–iii) and 'solitary' turbulent OS (see figure 6*c* i–iii) flow states, highly ordered coherent structures appearing as localized inflow streaks clearly show that significant polymer extension only occurs in the narrow axial zones occupied by OSs. As expected the localized strong inflows are more significant in the outer-wall region as compared to those in the inner-wall region, indicating larger instantaneous polymer extension in that region. Interestingly, for all the flow states the inflow/outflow streak patterns are similar in shape throughout the gap. The physics behind this similarity can be understood by considering the following scenario: (i) generation of significant 'hoop' stresses and a commensurate elastic body force in the outer-wall region that give rise to localized radial inflows; (ii) the radially inward velocity in turn accelerates in the outer half of the gap and achieves its maximum near the gap centre; and (iii) finally, the radial inward velocity decelerates due to the adverse radial pressure gradient and the centrifugal force in the inner half of the gap. For all three flow states, i.e. inertio-elastic turbulence, flame-like turbulent OSs and 'solitary' turbulent OS flow states, our simulation results support this scenario. Specifically, the maximum radial velocity is realized near the gap centre, i.e. 0.05, 0.04 and 0.03 for the inertio-elastic turbulence, the flame-like turbulent OSs and 'solitary' turbulent OS flow states, respectively. Therefore, the time scale for a fluid element travelling radially through the gap is $\sim 0.8\lambda$, λ and 1.3λ for these three flow states. This time scale is much smaller than the typical time scale of the space–time flow patterns shown in figure 1. Thus, the localized coherent structures arising near the outer wall can be advected across the gap without significant modification as such modifications occur at much longer time scales.

A close examination of the inflow/outflow streaks (see figure 6*a* i–iii) also clearly points to the radial delineation of the flow domain into three regions with distinct flow characteristics: a fluid-inertia (or outflow-) dominated regime near the inner wall, a polymer-elasticity (or inflow-) dominated regime near the outer wall, and an

inflow/outflow regime in the core region. Consequently in the inertio-elastic turbulence state ($Re = 250$), fluid elements travelling from inner- to outer-wall regions experience a transition from an outflow- to an inflow-dominated regime. Close to the inner wall, the change in u_r-PDF asymmetry (see figure 5) and the resulting inflow/outflow patterns (see figure 6) suggest a similar flow transition as Re is reduced from 250 to 10. Specifically, at the middle of the gap and near the inner wall, the flow dynamics is fluid inertia dominated at high $Re[=250]$, and polymeric elasticity dominated at low $Re[=10]$, i.e. the 'solitary' turbulent OS state.

4. Conclusions

The first DNS of elastically induced turbulence in the Taylor–Couette flow has been reported. Specifically, a key feature of elastically induced turbulent flows, namely, the broad continuous power-law-decay regions spanning more than two orders of magnitude in frequency, has been accurately captured by our simulations. Moreover, for the inertio-elastic turbulence state, three distinct flow domains in the gap have been identified for the first time, i.e. a fluid-inertia (or outflow-) dominated inner-wall region, a fluid-elasticity (or inflow-) dominated outer-wall region, and an inflow/outflow core region. Finally, a simple mechanism for elastically induced transition to a turbulent flow state in TC flow based on the variation of elastic body and inertial forces across the gap has been postulated. In turn, the applicability of this simple mechanism to other elastically modified TC flow states such as the flame-like turbulent OS and 'solitary' turbulent OS has been indicated.

Acknowledgements

References

AL-MUBAIYEDH, U. A., SURESHKUMAR, R. & KHOMAMI, B. 1999 Influence of energetics on the stability of viscoelastic Taylor–Couette flow. *Phys. Fluids* **11**, 3217–3226.

AL-MUBAIYEDH, U. A., SURESHKUMAR, R. & KHOMAMI, B. 2000 Linear stability of Taylor–Couette flow: influence of fluid rheology and energetics. *J. Rheol.* **44**, 1121–1138.

AVGOUSTI, M. & BERIS, A. N. 1993 Viscoelastic Taylor–Couette flow: Bifurcation analysis in the presence of symmetries. *Proc. R. Soc. Lond.* A **443**, 17–37.

BAUMERT, B. M. & MULLER, S. J. 1997 Flow regimes in model viscoelastic fluids in a circular Couette system with independently rotating cylinders. *Phys. Fluids* **9**, 566–586.

BAUMERT, B. M. & MULLER, S. J. 1999 Axisymmetric and non-axisymmetric elastic and inertio-elastic instabilities in Taylor–Couette flow. *J. Non-Newtonian Fluid Mech.* **83**, 33–69.

BERTI, S., BISTAGNINO, A., BOFFETTA, G., CELANI, A. & MUSACCHIO, S. 2008 Two-dimensional elastic turbulence. *Phys. Rev.* E **77**, 055306(R).

BERTI, S. & BOFFETTA, G. 2010 Elastic waves and transition to elastic turbulence in a two-dimensional viscoelastic kolmogorov flow. *Phys. Rev.* E **82**, 036314.

BONN, D., INGREMEAU, F., AMAROUCHENE, Y. & KELLAY, H. 2011 Large velocity fluctuations in small-Reynolds-number pipe flow of polymer solutions. *Phys. Rev.* E **84**, 045301.

BURGHELEA, T., SEGRE, E. & STEINBERG, V. 2007 Elastic turbulence in von Kármán swirling flow between two disks. *Phys. Fluids* **19**, 053104.

DUTCHER, C. S. & MULLER, S. J. 2009 The effects of drag reducing polymers on flow stability insights from the Taylor–Couette problem. *Korea-Australia Rheol. J.* **21**, 213–223.

DUTCHER, C. S. & MULLER, S. J. 2011 Effects of weak elasticity on the stability of high Reynolds number co- and counter-rotating Taylor–Couette flows. *J. Rheol.* **55**, 1271–1295.

DUTCHER, C. S. & MULLER, S. J. 2013 Effects of moderate elasticity on the stability of co- and counter-rotating Taylor–Couette flows. *J. Rheol.* **57**, 791–812.

GROISMAN, A. & STEINBERG, V. 1996 Couette–Taylor flow in a dilute polymer solution. *Phys. Rev. Lett.* **77**, 1480–1483.

GROISMAN, A. & STEINBERG, V. 1997 Solitary vortex pairs in viscoelastic Couette flow. *Phys. Rev. Lett.* **78**, 1460–1463.

GROISMAN, A. & STEINBERG, V. 1998 Mechanism of elastic instability in Couette flow of polymer solutions: experiment. *Phys. Fluids* **10**, 2451–2463.

GROISMAN, A. & STEINBERG, V. 2004 Elastic turbulence in curvilinear flows of polymer solutions. *New J. Phys.* **6**, 29.

JUN, Y. G. & STEINBERG, V. 2011 Elastic turbulence in a curvilinear channel flow. *Phys. Rev. E* **84**, 056325.

KUMAR, K. A. & GRAHAM, M. D. 2000 Solitary coherent structures in viscoelastic shear flow: Computation and mechanism. *Phys. Rev. Lett.* **85**, 4056–4059.

LARSON, R. G. 1992 Instabilities in viscoelastic flows. *Rheol. Acta* **31**, 213–263.

LARSON, R. G., SHAQFEH, E. S. G. & MULLER, S. J. 1990 A purely elastic transition in Taylor–Couette flow. *J. Fluid Mech.* **218**, 573–600.

LATRACHE, N., CRUMEYROLLE, O. & MUTABAZI, I. 2012 Transition to turbulence in a flow of a shear-thinning viscoelastic solution in a Taylor–Couette cell. *Phys. Rev. E* **86**, 056305.

LI, C. F., SURESHKUMAR, R. & KHOMAMI, B. 2006 Influence of rheological parameters on polymer induced turbulent drag reduction. *J. Non-Newtonian Fluid Mech.* **140**, 23–40.

SHAQFEH, E. S. G. 1996 Purely elastic instabilities in viscometric flows. *Annu. Rev. Fluid Mech.* **28**, 129–185.

SU, Y. Y. & KHOMAMI, B. 1992 Numerical solution of eigenvalue problems using spectral techniques. *J. Comput. Phys.* **100**, 297–305.

SURESHKUMAR, R. & BERIS, A. N. 1995 Effect of artificial stress diffusivity on the stability of numerical calculations and the dynamics of time-dependent viscoelastic flows. *J. Non-Newtonian Fluid Mech.* **60**, 53–80.

SURESHKUMAR, R., BERIS, A. N. & AVGOUSTI, M. 1994 Non-axisymmetric subcritical bifurcations in viscoelastic Taylor–Couette flow. *Proc. R. Soc. Lond.* A **447**, 135–153.

THOMAS, D. G., AL-MUBAIYEDH, U. A., SURESHKUMAR, R. & KHOMAMI, B. 2006*a* Time-dependent simulations of non-axisymmetric patterns in Taylor–Couette flow of dilute polymer solutions. *J. Non-Newtonian Fluid Mech.* **138**, 111–133.

THOMAS, D. G., KHOMAMI, B. & SURESHKUMAR, R. 2009 Nonlinear dynamics of viscoelastic Taylor–Couette flow: effect of elasticity on pattern selection, molecular conformation and drag. *J. Fluid Mech.* **620**, 353–382.

THOMAS, D. G., SURESHKUMAR, R. & KHOMAMI, B. 2006*b* Pattern formation in Taylor–Couette flow of dilute polymer solutions: dynamical simulations and mechanism. *Phys. Rev. Lett.* **97**, 054501.

WHITE, J. M. & MULLER, S. J. 2000 Viscous heating and the stability of Newtonian and viscoelastic Taylor–Couette flows. *Phys. Rev. Lett.* **84**, 5130–5133.

WHITE, J. M. & MULLER, S. J. 2002*a* Experimental studies on the stability of Newtonian Taylor–Couette flow in the presence of viscous heating. *J. Fluid Mech.* **462**, 133–159.

WHITE, J. M. & MULLER, S. J. 2002*b* The role of thermal sensitivity of fluid properties, centrifugal destabilization, and nonlinear disturbances on the viscous heating instability in Newtonian Taylor–Couette flow. *Phys. Fluids* **14**, 3880–3890.

ZHANG, H. N., LI, F. C., CAO, Y., TOMOAKI, K. & YU, B. 2013 Direct numerical simulation of elastic turbulence and its mixing-enhancement effect in a straight channel flow. *Chin. Phys.* B **22**, 024703.